[4]G. D. Mahan and J. J. Hopfield, Phys. Rev. Letters 12, 241 (1964).
[5]Yukio Osaka, J. Phys. Soc. Japan 19, 2347 (1964).
[6]David M. Larsen, Phys. Rev. 142, 428 (1966).
[7]M. Saitoh and A. Kawabata, J. Phys. Soc. Japan 23, 1006 (1967).
[8]George Whitfield, Bull. Am. Phys. Soc. 10, 388 (1965).
[9]Meheryar Engineer and George Whitfield, Phys. Rev. 179, 869 (1969).
[10]Wayne E. Tefft, Phys. Rev. 164, 1032 (1967).
[11]S. I. Pekar, *Research in Electron Theory of Crystals* (United States Atomic Energy Commission, Division of Technical Information, Washington, D. C., 1963), translation series No. AEC-tr-5575 Physics.
[12]N. N. Bogoliubov and S. V. Tiablikov Zh. Eksperim. i Teor. Fiz., 19, 256 (1949).
[13]G. R. Allcock, Ref. 1, p. 45.
[14]G. Höhler, Nuovo Cimento 2, 691 (1955).
[15]T. D. Schultz, Ref. 1, p. 92.
[16]These divergences were independently noticed by D. Matz.
[17]$\gamma = 0.577\cdots$ is Euler's constant $E_1(Z) = \int_z^\infty dt\, e^{-t}/t$ $|\arg z| < \pi$, a form of the exponential integral. See *Handbook of Mathematical Functions*, Natl. Bur. Std. Appl. Math. Series 55, (U. S. GPO, Washington, D. C., 1964).
[18]A. A. Kiyukanov and E. P. Pokatilov, Phys. Status Solidi 39, 277 (1970).

PHYSICAL REVIEW B VOLUME 6, NUMBER 10 15 NOVEMBER 1972

Effect of Uniaxial Stresses on the ^4E Level of a $3d^5$ Ion in Tetrahedral Symmetry: Study of Mn^{++} in ZnS

R. Parrot
Laboratoire de Luminescence II, Université de Paris VI, 11, quai Saint Bernard, Paris 5°, France

and

C. Blanchard
Laboratoire d'Electronique, Université de Provence, Faculté des Sciences de Saint-Jêrôme, Marseille 13°, France

(Received 22 February 1972)

The fine structure of the lines appearing in the 21 500-cm^{-1} absorption band of Mn^{++} in ZnS has been studied in great detail. We show that the three sharp zero-phonon lines at 21 242.5, 21 238, and 21 233.5 cm^{-1} are due to the transitions $^6A_1 \rightarrow \Gamma_6(^4E)$, $^6A_1 \rightarrow \Gamma_8(^4E)$, and $^6A_1 \rightarrow \Gamma_7(^4E)$ of Mn^{++} in T_d symmetry, the degeneracy of the ^4E level being lifted by the first-order effect of the spin-spin interaction and by the second-order effect of the spin-orbit interaction. To confirm these assignments, we performed a uniaxial-stress experiment on these levels by applying a pressure along the $[1\bar{1}0]$ crystallographic axis. We show that the observed splitting of the degenerate Γ_8 level (23×10^{-10} cm^{-1}/dyn) can be interpreted as being due to the combined action of the induced rhombic distortion and the spin-orbit interaction. Furthermore, we show that the other sharp phonon-assisted lines of the optical spectra behave like cubic Γ_6, Γ_8, and Γ_7 levels. Complementary studies regarding the polarization and intensities of these cubic lines have been performed in order to reinforce these interpretations. Finally, we studied the case of a pressure-induced trigonal distortion and the splitting of the ^4E level of Mn^{++} in the hexagonal phase.

I. INTRODUCTION

In luminescence the most studied $3d^5$ ion has been Mn^{++} incorporated as an activator in various A_{II}-B_{VI} compounds. However, until recently, the absence of good crystals prevented a systematic analysis of Mn^{++} energy levels in these compounds.

Generally, the energy levels of the Mn^{++} ion in T_d or O_h symmetry are determined using either the theoretical study carried out by Orgel[1] in a weak-field coupling scheme or the study made by Sugano and Tanabe[2] using an intermediate coupling scheme. In Fig. 1(a) we report some low-energy levels of the Mn^{++} ion calculated in an ionic model.

In 1965 and 1966, Langer *et al.*[3,4] studied the emission and absorption bands of ZnS:Mn, ZnSe:Mn, and CdS:Mn. They pointed out not only zero-phonon lines, but a certain number of phonon-assisted lines for all the bands. In addition, they established the origin of a great number of phonons participating in the emissions. For Mn^{++} in ZnS and ZnSe, they deduced the values for the cubic field parameter Dq and the Racah parameters B and C from the experimental spectra. For Mn^{++} in CdS, only the level $^4T_1$ can be observed, thus the optical parameters cannot be determined from experiments. However, while indicating the original multiplets of the observed zero-phonon lines, these authors did not explain their structure.

Amongst all the structures observed in ZnS:Mn, we studied those appearing in the band $^6A_1 \rightarrow {}^4E$

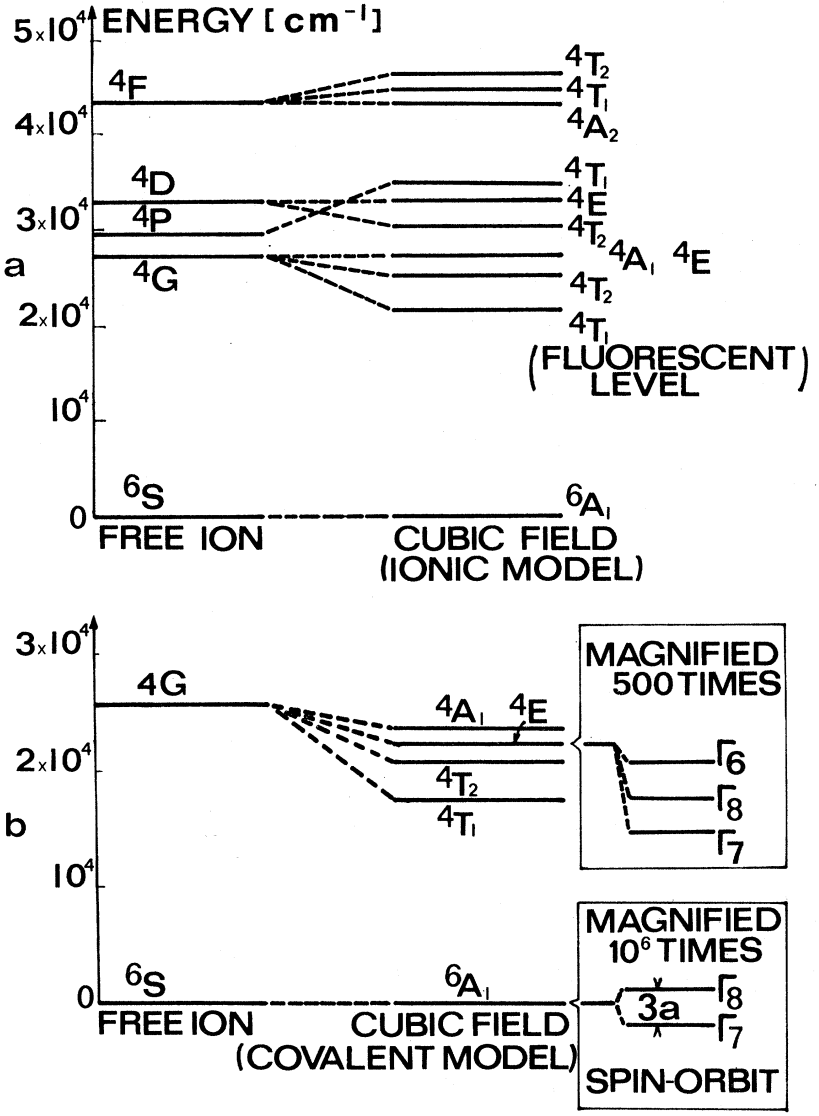

FIG. 1. Lowest energy levels for Mn^{++} in ZnS. (a) Levels in an ionic model where levels ^4E and $^4A_1$ are degenerate. (b) Splitting of levels ^4E and $^4A_1$ by covalency. The levels studied in this paper are given in the insert of (b). The splitting of the levels is shown on an expanded scale.

(21 500 cm^{-1}) and particularly, the structure of the zero-phonon line (21 238 cm^{-1}), which appears to be composed of three lines separated by 4.5 cm^{-1} [Fig. 2(a)]. Simple symmetry considerations show that these lines can be associated with the three levels $\Gamma_8(^4E)$, $\Gamma_7(^4E)$, and $\Gamma_6(^4E)$. The difficulty that we encounter is that the level $^4A_1$ does not appear in this description of the zero-phonon line. In fact, Koide and Pryce[5] have shown that the degeneracy of the levels ^4E and $^4A_1$ of Mn^{++} is lifted by covalency in the case of an octahedral symmetry. By adapting their findings to the case of a tetrahedral symmetry, we show that covalency can lift the degeneracy of levels ^4E and $^4A_1$ of Mn^{++} in ZnS [Fig. 1(b)].

To support our interpretation of the structure of level ^4E, we ran experiments under uniaxial stresses by applying a pressure parallel to the crystallographic axes $[1\bar{1}0]$ and [111]. In the first case ($\vec{P} \parallel [1\bar{1}0]$) we obtained evidence that the degeneracy of level $\Gamma_8(^4E)$ can be lifted by the pressure-induced rhombic distortion. In the second case ($\vec{P} \parallel [111]$), applied pressures were not sufficient to permit an experimental observation of the splitting of level $\Gamma_8(^4E)$ by the pressure-induced trigonal distortion. These experiments, as well as polarization experiments, are reported in Sec. II.

In the theoretical section, Sec. III, we study the effect of covalency on levels $^4A_1$ and ^4E, showing that these levels can be split in the case of a T_d symmetry. We demonstrate that the splitting of the ^4E level ($^4E \rightarrow \Gamma_6$, Γ_7, Γ_8) is due both to the spin-spin interaction and spin-orbit interaction

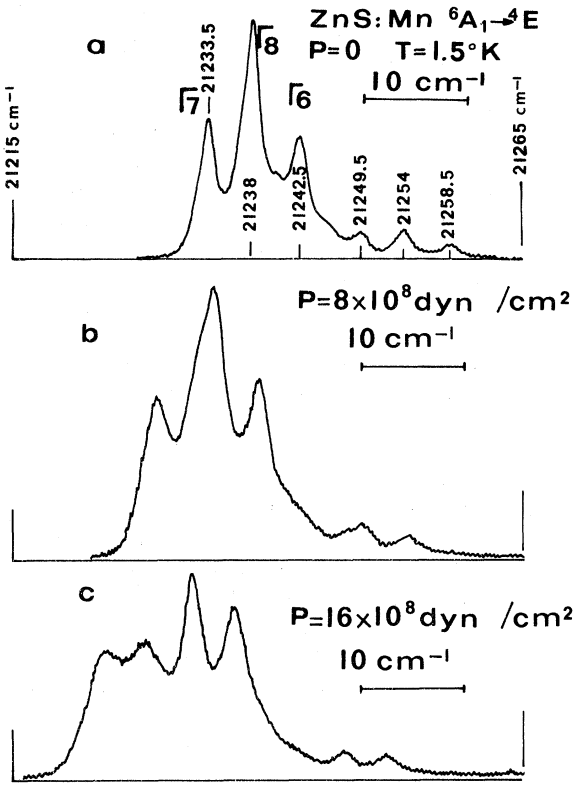

FIG. 2. Spectrometer recordings of some ZnS: Mn lines of the 21 500 cm^{-1} excitation band for applied pressure parallel to the [1$\bar{1}$0] direction. In (b) a splitting of the central line at 21 235 and 21 250 cm^{-1} becomes apparent as well as a shift of all lines toward lower energies. In (c) the preceding lines are well separated. The two lines at 21 243 and 21 240.3 cm^{-1} appearing in spectrum (a) have not been interpreted. All spectra were taken at 1.5 °K.

when $\vec{P}=0$, and also to the pressure-induced rhombic field when $\vec{P} \parallel [1\bar{1}0]$. The dipole strengths and polarization effects are studied theoretically. Finally, we give a calculation of the splitting of the ^4E level when pressure is applied along the [111] crystallographic axis.

In Sec. IV we compare the theoretical and experimental results.

II. EXPERIMENTS

A. Samples and Apparatus

For our experiments we used single crystals of ZnS of both hexagonal and cubic structure grown by Eagle Picher. As determined from electron-paramagnetic-resonance (EPR) spectra, the concentration was approximately 0.1–0.01 mol% Mn^{++} These spectra also showed that our samples were predominantly cubic with a 10% hexagonal phase, and that they presented also a number of Mn^{++} ions in other axial sites. The crystals which served for the uniaxial-stress experiments were sliced and mechanically polished, great attention being given to the faces perpendicular to the pressure. An interferometer controlled the parallelism of these faces during the polishing so that the distance between the two faces was determined with a margin of error less than 1 μ. The dimensions of one of the crystals were 8.25×2.85×1.55 mm; the cross-sectional area perpendicular to the [1$\bar{1}$0] direction was (2.85±0.01)×(1.55±0.01) mm. The dimensions of the other crystal used in our experiments were 5.00×1.25×0.82 mm; the cross-sectional area perpendicular to the [111] direction was (1.25±0.01)×(0.82±0.01) mm.

The stress rig was the same as that used by Schawlow *et al.*[6] except for the removal of the Teflon pedestal. The experiments were performed either at 1.5 or at 4.2 °K in a glass Dewar, the sample being directly immersed in liquid helium. The measurements were performed with a high-resolution spectrometer (HRS-2, manufactured by Jobin-Yvon) equipped with a grating having 1200 lines/mm. Almost all spectra were obtained with a resolution better than 0.4 cm^{-1} in the investigated region.

B. Experimental Results

We studied the behavior of the nine sharp lines appearing in the spectra near 21 238 cm^{-1} (group *A*), 21 254 cm^{-1} (group *B*), and 21 322 cm^{-1} (group *C*). Figure 2 shows the recordings at three different pressures ($\vec{P} \parallel [1\bar{1}0]$) for the *A* and *B* groups. For $\vec{P}=0$, the spectra are very similar to those of Langer and Ibuki.[3] For $P=8\times10^8$ dyn/cm^2 and $P=16\times10^8$ dyn/cm^2, a splitting of the central lines is apparent as well as a shift of the set of lines. In Fig. 3, displacements have been plotted in terms of pressure for the six lines of groups *A* and *B*. We see that the lines of the two groups have the same behavior in terms of pressure. The dashed line in this figure indicates the theoretical displacement of one small line whose peak cannot be determined experimentally since it is situated on the side of a line of strong amplitude of group *A*. The lines for group *C* being well isolated, we determined experimentally the positions of each of the lines for this group for applied pressure up to 16×10^8 dyn/cm^2. We have found that the behavior under pressure for the three lines of group *C* is identical to the behavior of the lines of group *A* (same splitting and shift in terms of pressure).

Further experiments on the effect of polarization on the nine lines studied showed that all the lines which appear at each group were polarized. In Fig. 4 we give the spectra for $P=16\times10^8$ dyn/cm^2 for group *A* and group *C*. Unfortunately, under high pressure, the lines of group *B* are too weak to be analyzed in detail and are partly super-

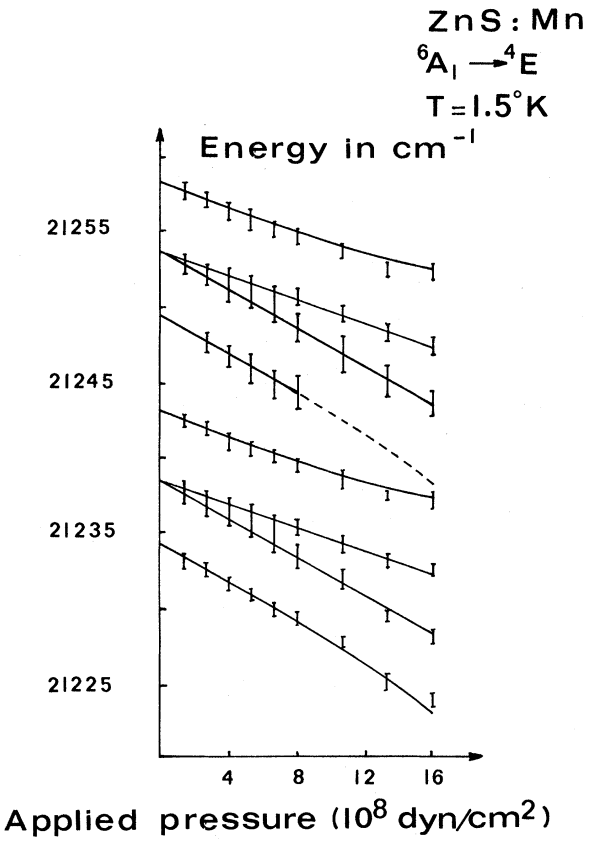

FIG. 3. Splitting and shift in function of applied pressure of the six lines of Fig. 2. $T = 1.5$ °K, pressure $\vec{P} \parallel [1\bar{1}0]$.

imposed with lines of group A. However, the two lines at higher energy of group B behave like the corresponding lines of group A.

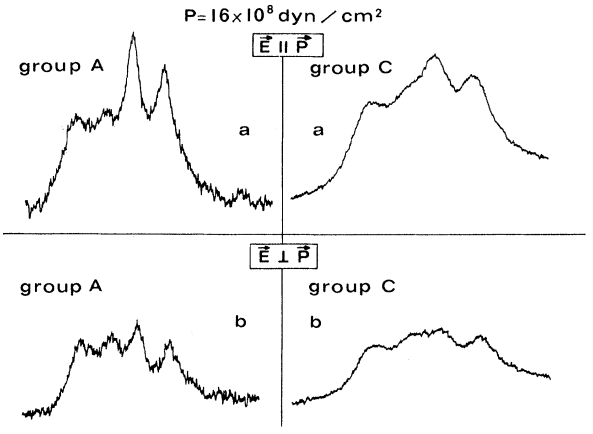

FIG. 4. Polarization effects for $\vec{P} \parallel [1\bar{1}0]$. (a) Electric field parallel to $[1\bar{1}0]$; (b) Electric field perpendicular to $[1\bar{1}0]$. The detailed geometry is given in Sec. IV of the text.

Experiments were performed with $\vec{P}$ parallel to the crystallographic axis $[111]_W$ common to the two different cubic centers present in our sample (Fig. 5). In this case we observed a broadening of the central line and a spreading of the lateral lines for groups A, B, and C (Fig. 6). In addition, all the lines were shifted linearly towards lower energy, but the shifts of the centers of gravity were different: 17.1 cm^{-1} for group A, 15.3 cm^{-1} for group B, and 14.6 cm^{-1} for group C for a maximum applied pressure $P = 36 \times 10^8$ dyn/cm^2. A simple interpretation is to relate the broadening of the central line to a splitting of level Γ_8 rather than to a nonuniform distribution of internal stresses since lines corresponding to levels Γ_6 and Γ_7 are not broadened.

Experiments made with polarized light show that the effects are the same for the lines of each group A, B, and C; however, the effect is not very sharp for group B given the smallness of the lines. In Fig. 7 we report spectra for $P = 36 \times 10^8$ dyn/cm^2 ($\vec{P} \parallel [111]_W$).

In order to recognize the line corresponding to the $^6A_1 \rightarrow {}^4A_1$ transition, we very carefully analyzed a large region around the $^6A_1 \rightarrow {}^4E$ band by running an experiment with pressure and another without

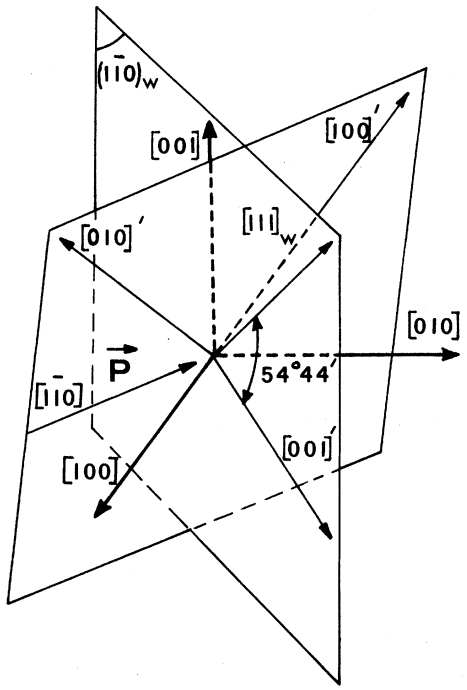

FIG. 5. Geometry for the cubic sites in ZnS. The crystallographic axes [100]', [010]', and [001]' of one site are obtained by rotating, around the $[111]_W$ axis, the crystallographic axes of the other site. The parameters of the spin Hamiltonian are identical for the two sites (Ref. 15).

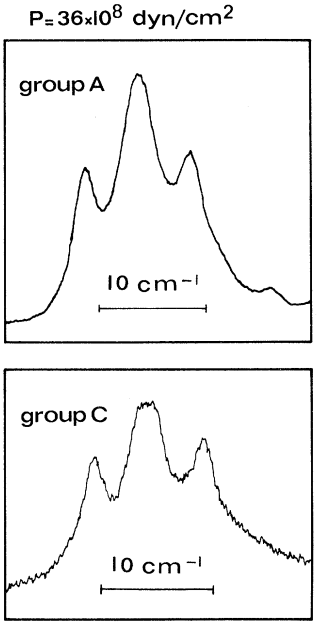

FIG. 6. Broadening of the central lines when $\vec{P} \parallel [111]_W$. $T = 1.5\,°K$. The light was unpolarized.

pressure. In the absence of pressure, the $^6A_1 \rightarrow {}^4A_1$ transition should give a single level $\Gamma_8(^4A_1)$ for the centers in cubic symmetry and could give two Kramers doublets in the case of a C_{3v} symmetry. (We considered this possibility since our crystal contained hexagonal centers, although only 10% of Mn^{++} centers are situated in sites of hexagonal symmetry.) By applying a pressure, only the degeneracy of the cubic level Γ_8 could be lifted. Not one particular experimental fact permitted us to attribute any of the lines appearing between 5000 (20 000 cm^{-1}) and 4200 Å (23 810 cm^{-1}) to level $^4A_1$. In particular, the behaviors of the sharp lines of each of the groups A, B, and C under uniaxial stress are too much alike to enable us to attribute one or two lines of one group to the $^6A_1 \rightarrow {}^4A_1$ transition.

III. THEORY

A. Splitting of Levels $^4A_1$ and ^4E

As indicated in Sec. I, the levels $^4A_1$ and ^4E are degenerate if only the ionic approximation is considered. We follow the arguments of Koide and Pryce[5] to show that covalency can remove the degeneracy of levels $^4A_1$ and ^4E in the case of tetrahedral symmetry.

As the main part of the Coulomb integrals comes from the charge clouds near the nucleus of the central atom, we replace the radial part of the $|3t_2\rangle$ electronic wave functions by k times the original ones since they are the only ones which mix with the σ orbitals of the ligands. In this approximation the matrix of the electrostatic interaction for the states of ^4E symmetry is given in Table I, where $B' = B_0 k^2$, $B'' = B_0 k^4$, $C' = C_0 k^2$, $C'' = C_0 k^4$; B_0 and C_0 being the Racah parameters of the free ion. The energy of the state $t_2^3(^4A_2)e^2(^3A_2):(^4A_1)$ is $10B' + 5C'$. The notations are those of Koide and Pryce. The $^6A_1$ state is taken as reference.

Assuming $B_0 = 900\ cm^{-1}$ and $C_0 = 3600\ cm^{-1}$, we can find the value of k^2 by fitting the theoretical energy of the level $^4E(^4G)$ to the experiment. We obtain $k^2 = 0.84$ and $W(^4A_1) - W(^4E(^4G)) = 1300\ cm^{-1}$ for Mn^{++} in cubic ZnS.[7] In the following, the slight mixing of the levels $^4E(^4G)$ and $^4E(^4D)$ will be neglected.

TABLE I. Matrix of the electrostatic interaction for the states of ^4E symmetry. B', B'', C', and C'' are defined in Sec. III A.

^4E	$t_2^3(^2E)e^2(^3A_2)$	$t_2^3(^4A_2)e^2(^1E)$
$t_2^3(^2E)e^2(^3A_2)$	$4B' + 2C' + 9B'' + 3C''$	$-2\sqrt{3}\,B'$
$t_2^3(^4A_2)e^2(^1E)$	$-2\sqrt{3}\,B'$	$8B_0 + 2C_0 + 6B' + 3C'$

B. Levels in Undistorted Crystal Field of T_d Symmetry

The Hamiltonian governing the energy levels of a $3d^5$ ion in a site with T_d symmetry is of the form

$$\mathcal{H} = \mathcal{H}_0 + \mathcal{H}_c + \mathcal{H}_{so} + \mathcal{H}_{ss},$$

where $\mathcal{H}_0$ is the free-ion Hamiltonian and $\mathcal{H}_c$ is the Hamiltonian in a cubic field. $\mathcal{H}_{so}$ and $\mathcal{H}_{ss}$ are, respectively, the spin-orbit and spin-spin Hamiltonians. The levels of Mn^{++} in a cubic field have generally been calculated by omitting the interaction of the fundamental configuration with the excited configurations of opposite parity by the odd potentials. This hypothesis is acceptable since the Racah and crystal field parameters are obtained

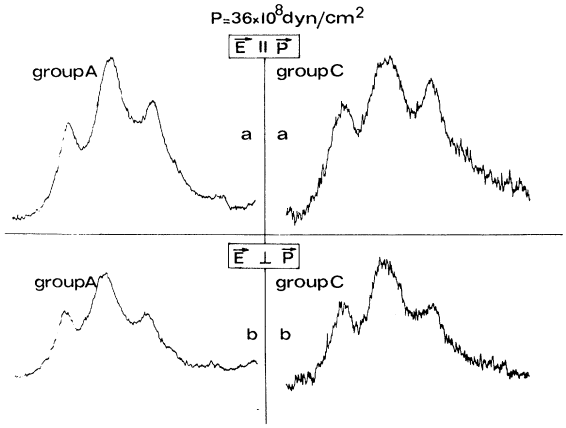

FIG. 7. Polarization effects for $\vec{P} \parallel [111]$. (a) Electric field parallel to $[111]_W$; (b) electric field perpendicular to $[111]_W$.

by fitting the experimental levels to the theoretical levels. To our knowledge, the spin-orbit interaction has not been previously studied in detail. Since Koide and Pryce[5] have given only qualitative explanations for the action of this interaction on the ^4E level, our first aim will be to give a detailed analysis of it.

The first-order effect of the spin-orbit interaction, as can easily be seen, cannot lift the degeneracy of the ^4E level. We must take into account the spin-orbit interaction to the second order, coupling the ^4E level to the T_1 and T_2 levels, in order to get the following decomposition:

$$^4E \rightarrow \Gamma_6 + \Gamma_7 + \Gamma_8 .$$

In order to make full use of the symmetry properties we will work in the spinor symmetry group T_d^*. For calculation of the reduced matrix elements we will use the complex tetragonal component system defined by Griffith.[8,9]

The detailed calculations are given for the $^4T_1$ and $^4T_2$ levels which intervene in the calculations of the dipole strengths. The contributions of all the levels $^2T_1$, $^2T_2$, $^4T_1$, and $^4T_2$ are given in Table VII.

We can express the quadruplets $^4T_1$ and $^4T_2$ in spectroscopic terms $|L, M_L\rangle$ in the following manner:

$$|^4_i T_1 M_\Gamma\rangle = \alpha_i |^4P, T_1 M_\Gamma\rangle + \beta_i |^4F, T_1 M_\Gamma\rangle + \gamma_i |^4G, T_1 M_\Gamma\rangle ,$$

$$|^4_i T_2 M_\Gamma\rangle = \alpha'_i |^4D, T_2 M_\Gamma\rangle + \beta'_i |^4F, T_2 M_\Gamma\rangle + \gamma'_i |^4G, T_2 M_\Gamma\rangle .$$

The components u and v of level ^4E perturbed by $\mathcal{H}_{so}$ will be given by

$$|(^4E_u SM_S)'\rangle = |^4E_u SM_S\rangle + \sum_{i=1}^{3}\sum_{q=-1}^{+1} \frac{\beta_i \rho}{\Delta_i} \langle ^4F, T_{1q} SM_S - q| (-1)^q \times \sum_j l^1_{jq} s^1_{j-q} |^4G, E_u SM_S\rangle |^4_i T_{1q} M_S - q\rangle + \sum_{i=1}^{3}\sum_{q=+1,-1} \frac{\beta'_i \rho}{\Delta'_i} \langle ^4F, T_{2q} M_S - q| (-1)^q \times \sum_j l^1_{jq} s^1_{j-q} |^4G, E_u SM_S\rangle |^4_i T_{2q} M_S - q\rangle$$

and

$$|(^4E_v SM_S)'\rangle = |^4E_v SM_S\rangle + \sum_{i=1}^{3}\sum_{q=+1,-1} \frac{\beta_i \rho}{\Delta_i} \langle ^4F, T_{1q} SM_S - q| (-1)^q \times \sum_j l^1_{jq} s^1_{j-q} |^4G, E_v SM_S\rangle |^4_i T_{1q} M_S - q\rangle + \sum_{i=1}^{3}\sum_{q=+1}^{+1} \frac{\beta'_i \rho}{\Delta'_i} \langle ^4F, T_{2q} M_S - q| (-1)^q \times \sum_j l^1_{jq} s^1_{j-q} |^4G, E_v SM_S\rangle |^4_i T_{2q} M_S - q\rangle .$$

ρ is the spin-orbit constant. Δ_i and Δ'_i are the energy differences between the ^4E level and the $^4_i T_1$ and $^4_i T_2$ levels. $\mathcal{H}_{so}$ is expressed in terms of a scalar product of the monoelectronic tensor operators of rank 1, l^1_i and s^1_i:

$$\mathcal{H}_{so} = \rho \sum_{q=-1}^{+1} (-1)^q \sum_j l^1_{jq} s^1_{j-q} ,$$

where index j refers to the jth electron and q to the components of the tensors l^1 and s^1. It is very convenient to calculate

$$\langle (^4E_u SM_S)' | \mathcal{H}_{so} | (^4E_u S' M'_S)' \rangle$$

and

$$\langle (^4E_v SM_S)' | \mathcal{H}_{so} | (^4E_v S' M'_S)' \rangle$$

in the spinor group.

The matrix elements of $\mathcal{H}_{so}$ in the spinor group T_d^* are given by the following general relation:

$$\langle \Gamma M_\Gamma J \Gamma^* M_{\Gamma^*} S | \mathcal{H}_{so} | \Gamma' M_{\Gamma'} J' \Gamma^{*\prime} M_{\Gamma^{*\prime}} S' \rangle = \langle \Gamma S || \mathcal{H}_{so} || \Gamma' S' \rangle \Omega_{JJ'} \begin{pmatrix} S & S' & T_1 \\ \Gamma' & \Gamma & M_{\Gamma^*} \end{pmatrix} . \quad (1)$$

(In our case J or J' refer to representations Γ^* or $\Gamma^{*\prime}$ of the spinor group when they intervene more than once in the direct products $\Gamma \times T_1$ or $\Gamma' \times T_1$.) The $\Omega_{JJ'}$ are given by Griffith.[8] Some $\Omega_{JJ'}$ used in this section are given in Table II.

The energies of the levels Γ_6, Γ_7, and Γ_8 due to the spin-orbit interaction are calculated from the following values of the reduced matrix elements:

$$\langle ^4E(^4G) || \mathcal{H}_{so} || ^4T_1(^4F)\rangle = -\langle ^4T_1(^4F) || \mathcal{H}_{so} || ^4E(^4G)\rangle = +10/\sqrt{21} ,$$

$$\langle ^4E(^4G) || \mathcal{H}_{so} || ^4T_2(^4F)\rangle = -\langle ^4T_2(^4F) || \mathcal{H}_{so} || ^4E(^4G)\rangle = -2\sqrt{15}/\sqrt{7} .$$

TABLE II. Values of $\Omega_{JJ'}$ $(^{3/2}_{\Gamma'}\ ^{3/2}_{\Gamma}\ ^{T_1}_{M_{\Gamma^*}})$. The notations are those of Griffith (Ref. 8). The values of Ω_{JJ}, $(^{3/2}_{\Gamma'}\ ^{3/2}_{\Gamma}\ ^{T_1}_{M_{\Gamma^*}})$ are related to the preceding by $\Omega_{J'J}$ $(^{3/2}_{\Gamma}\ ^{3/2}_{\Gamma'}\ ^{T_1}_{M_{\Gamma^*}}) = (-1)^{\Gamma+\Gamma'}\Omega_{JJ'}$ $(^{3/2}_{\Gamma'}\ ^{3/2}_{\Gamma}\ ^{T_1}_{M_{\Gamma^*}})$, with $(-1)^{T_1} = -(-1)^{T_2} = -1$.

Γ_6	$^4T_1$	$^4T_2$	Γ_7	$^4T_1$	$^4T_2$	Γ_8	$^4T_2(\frac{3}{2})$	$^4T_2(\frac{5}{2})$
$^4T_1$	$+\frac{\sqrt{5}}{6\sqrt{2}}$	$+\frac{1}{2\sqrt{30}}$	$^4T_1$	$-\frac{1}{2\sqrt{10}}$	$-\frac{1}{2\sqrt{30}}$	$^4T_1(\frac{3}{2})$	$-\frac{\sqrt{2}}{5\sqrt{15}}$	$+\frac{2\sqrt{2}}{5\sqrt{15}}$
$^4T_2$	$-\frac{1}{2\sqrt{30}}$	$-\frac{1}{2\sqrt{10}}$	$^4T_2$	$+\frac{1}{2\sqrt{30}}$	$\frac{\sqrt{5}}{6\sqrt{2}}$	$^4T_1(\frac{5}{2})$	$+\frac{2\sqrt{2}}{5\sqrt{15}}$	$+\frac{3\sqrt{3}}{10\sqrt{10}}$

TABLE III. Values of $\Pi_{JJ'}(\Gamma''M_{\Gamma''}\Gamma\Gamma^*M_{\Gamma^*}\Gamma'\Gamma'^*M_{\Gamma'^*})$. The values of J and J' are given in parentheses.

T_{20}	${}^4E\Gamma_7\frac{1}{2}$	${}^4E\Gamma_8-\frac{3}{2}$	T_{20}	${}^4E\Gamma_8\frac{1}{2}$	T_{20}	${}^4E\Gamma_6\frac{1}{2}$
${}^4T_1\Gamma_6\frac{1}{2}$	$+\frac{1}{3\sqrt{2}}$	$+\frac{1}{3\sqrt{2}}$	${}^4T_1\Gamma_7\frac{1}{2}$	$+\frac{1}{3\sqrt{2}}$	${}^4T_1\Gamma_7\frac{1}{2}$	$+\frac{1}{3\sqrt{2}}$
${}^4T_2\Gamma_6\frac{1}{2}$	$-\frac{1}{3\sqrt{2}}$	$+\frac{1}{3\sqrt{2}}$	${}^4T_2\Gamma_7\frac{1}{2}$	$-\frac{1}{3\sqrt{2}}$	${}^4T_2\Gamma_7\frac{1}{2}$	$+\frac{1}{3\sqrt{2}}$
${}^4T_1(\frac{5}{2})\frac{1}{2}$	$-\frac{1}{\sqrt{10}}$	$-\frac{1}{\sqrt{10}}$	${}^4T_1(\frac{5}{2})-\frac{3}{2}$	$-\frac{1}{3\sqrt{10}}$	${}^4T_1(\frac{5}{2})-\frac{3}{2}$	$-\frac{1}{3\sqrt{10}}$
${}^4T_1(\frac{3}{2})\frac{1}{2}$	$-\frac{1}{3\sqrt{10}}$	$-\frac{1}{3\sqrt{10}}$	${}^4T_1(\frac{3}{2})-\frac{3}{2}$	$+\frac{1}{\sqrt{10}}$	${}^4T_1(\frac{3}{2})-\frac{3}{2}$	$+\frac{1}{\sqrt{10}}$
${}^4T_2(\frac{5}{2})\frac{1}{2}$	$+\frac{1}{3\sqrt{10}}$	$-\frac{1}{3\sqrt{10}}$	${}^4T_2(\frac{3}{2})-\frac{3}{2}$	$-\frac{1}{\sqrt{10}}$	${}^4T_2(\frac{3}{2})-\frac{3}{2}$	$+\frac{1}{\sqrt{10}}$
${}^4T_2(\frac{3}{2})\frac{1}{2}$	$+\frac{1}{\sqrt{10}}$	$+\frac{1}{\sqrt{10}}$	${}^4T_2(\frac{3}{2})-\frac{3}{2}$	$-\frac{1}{3\sqrt{10}}$	${}^4T_2(\frac{3}{2})-\frac{3}{2}$	$+\frac{1}{3\sqrt{10}}$

From these values and from the Ω's we get

$$W(\Gamma_6)=\tfrac{5}{126}K_1+\tfrac{9}{14}K_2\,,$$

$$W(\Gamma_7)=\tfrac{45}{126}K_1+\tfrac{1}{14}K_2\,,$$

$$W(\Gamma_8)=\tfrac{25}{126}K_1+\tfrac{5}{14}K_2\,,$$

with

$$K_1=\sum_i \frac{\beta_i^2}{\Delta_i}\rho^2$$

and

$$K_2=\sum_i \frac{\beta_i'^2}{\Delta_i}\rho^2\quad.$$

In order to account for the spin-spin interaction to the first order, we use the equivalent Hamiltonian calculated by Pryce[10]:

$$\mathcal{H}_{\text{ss eq}}=+p\,[(\vec{L}\cdot\vec{S})^2+\tfrac{1}{2}(\vec{L}\cdot\vec{S})-\tfrac{1}{3}L(L+1)S(S+1)],$$

with $p=-0.334\ \text{cm}^{-1}$. This operator is diagonal in $T_d{}^*$. Explicitly, we get

$$W(\Gamma_6)-W(\Gamma_8)=W(\Gamma_8)-W(\Gamma_7)=-8p\,.$$

C. Levels in the Distorted Crystal Field $\vec{P}\parallel[1\bar{1}0]$

We shall consider the case of a pressure $\vec{P}$ applied along the $[1\bar{1}0]$ crystallographic axis of a cubic sample and show that the degeneracy of level Γ_8 is lifted.

For T_d symmetry, it is convenient to express the variation ΔV of the crystal field in terms of the linear combinations $\epsilon(\Gamma, M_\Gamma)$ of the components of the stress tensor spanning the irreducible representations Γ of the symmetry group. Thus, by using the coupling coefficients defined by Griffith,[8] we get

$$\Delta V=\sum_{\Gamma M_\Gamma}[\lambda(\Gamma)]^{1/2}V(\Gamma,M_\Gamma)\,\epsilon(\Gamma,M_\Gamma)\,.$$

In this expression, $\lambda(\Gamma)$ is the dimension of the representation Γ, and $V(\Gamma, M_\Gamma)$ is an operator spanning the component M_Γ of the representation Γ.

For $\vec{P}\parallel[1\bar{1}0]$ the nonzero linear combinations of the stress tensor coefficients are

$$\epsilon(A_1)=(s_{11}+2s_{12})P\,,$$

$$\epsilon(E_u)=-(s_{11}-s_{12})P\,,$$

$$\epsilon(T_{2\zeta})=+s_{44}P/2\,,$$

where s_{ij}'s are elastic compliance factors of the crystal.

It is easy to see that there is no first-order effect of these deformations on Γ_6, Γ_7, and Γ_8. The splitting of the Γ_8 level is due principally to a second-order perturbation mixing the ${}^4E$ level with the T_1 and T_2 levels via the rhombic deformations $\epsilon(T_2)$ and the spin-orbit coupling.

In order to calculate the matrix elements of ΔV in $T_d{}^*$, it is convenient to use the following relation which is the counterpart of relation (1) for a spin-independent operator:

$$\langle\Gamma J\Gamma^*M_{\Gamma^*}|\,V(\Gamma''M_{\Gamma''})\,|\Gamma'J'\Gamma^{*\prime}M_{\Gamma^{*\prime}}\rangle$$
$$=\langle\Gamma\|V\Gamma''\|\Gamma'\rangle\times\Pi_{JJ'}(\Gamma''M_{\Gamma''}\Gamma^*M_{\Gamma^*}\Gamma'\Gamma^{*\prime}M_{\Gamma^{*\prime}})\,,$$

with

$$\Pi_{JJ'}(\Gamma''M_{\Gamma''}\Gamma\Gamma^*\Gamma'\Gamma^{*\prime})=\sum_{M_S M_\Gamma M_{\Gamma'}}(-1)^{\Gamma^*+M_\Gamma}\times V\begin{pmatrix}\Gamma & \Gamma' & \Gamma''\\ -M_\Gamma & M_{\Gamma'} & M_{\Gamma''}\end{pmatrix}\times\langle S\Gamma J\Gamma^*M_{\Gamma^*}|\,S\Gamma M_S M_\Gamma\rangle\times\langle S\Gamma' M_S M_{\Gamma'}|\,S\Gamma' J'\Gamma^{*\prime}M_{\Gamma^{*\prime}}\rangle\,.$$

The Π's intervening in our calculations are given in Table III.

Taking into account ΔV and $\mathcal{H}_{so}$ we get the matrix elements given in Table IV. The energy of the unperturbed Γ_8 level is taken as reference. The eigenvalues of this 8×8 matrix are $\pm\frac{1}{2}|Z|$ and $\pm\frac{3}{2}(X^2+|Z|^2)^{1/2}$ with

TABLE IV. Matrix elements of the pressure-induced crystal field and of the spin-orbit interaction when $\vec{P}\parallel[1\bar{1}0]$. X and Z are defined in Sec. III C.

	$\Gamma_6\pm\frac{1}{2}$	$\Gamma_7\pm\frac{1}{2}$	$\Gamma_8\mp\frac{3}{2}$	$\Gamma_8\pm\frac{1}{2}$
$\Gamma_6\pm\frac{1}{2}$	$-\frac{3}{2}X$	$\mp\frac{1}{2}Z$	$+Z$	0
$\Gamma_7\pm\frac{1}{2}$	$\mp\frac{1}{2}Z^*$	$+\frac{3}{2}X$	0	$+Z$
$\Gamma_8\mp\frac{3}{2}$	$+Z^*$	0	0	$\mp\frac{1}{2}Z$
$\Gamma_8\pm\frac{1}{2}$	0	$+Z^*$	$\mp\frac{1}{2}Z^*$	0

$$Z=\frac{2i\sqrt{5}}{3\sqrt{21}}\,\rho\Big(\langle E_v|\,\Delta V(T_{20})|\,T_{10}(F)\rangle\sum_i\frac{\beta_i^2}{\Delta_i}+\langle E_v|\,\Delta V(T_{20})|\,T_{10}(P)\rangle\sum_i\frac{\alpha_i\beta_i}{\Delta_i}\Big)+\frac{2i}{\sqrt{21}}\,\rho\,\langle E_u|\,\Delta V(T_{20})|\,T_{20}(F)\rangle\sum_i\frac{\beta_i'^2}{\Delta_i'}$$

and

$$X=+\tfrac{40}{189}K_1+\tfrac{8}{21}K_2\ .$$

D. Dipole Strengths: Polarization

First, we shall consider the case of an unstressed crystal. For the sake of brevity the calculations will be made only for the zero-phonon transitions.

For a $3d^5$ ion in a T_d symmetry site, the relevant part of the Hamiltonian is

$$\mathcal{H}=\mathcal{H}_0+\mathcal{H}_{even}+\mathcal{H}_{so}+\mathcal{H}_{eq}\ ,$$

$\mathcal{H}_{even}$ being the even part of the cubic crystal potential. $\mathcal{H}_{eq}$ is an equivalent even operator arising, in our case, from the composition of the electric dipole moment operator $\vec{\mathfrak{M}}$ with the odd part of the crystal potential, $\mathcal{H}_{odd}$. $\mathcal{H}_{eq}$ is given by[11]

$$\mathcal{H}_{eq}=\sum_{\Psi_{odd}}\frac{\vec{\mathfrak{M}}\,|\Psi_{odd}\rangle\langle\Psi_{odd}|\mathcal{H}_{odd}+\mathcal{H}_{odd}|\Psi_{odd}\rangle\langle\Psi_{odd}|\vec{\mathfrak{M}}}{E(3d^5)-E(\Psi_{odd})}\ ,$$

$|\Psi_{odd}\rangle$ being the wave function of an opposite-parity configuration $(3d^4n'l')$. It is convenient to write $\vec{\mathfrak{M}}$ in terms of tensor operators of rank 1:

$$\vec{\mathfrak{M}}=-e(-D^1_{-1}\vec{k}^{+}-D^1_1\vec{k}^{-}+D^1_0\vec{k}^{0})\ ,$$

with

$$\vec{k}^{+}=\frac{-\vec{i}+i\vec{j}}{\sqrt{2}}\ ,\qquad \vec{k}^{-}=\frac{\vec{i}-i\vec{j}}{\sqrt{2}}\ ,\qquad \vec{k}^{0}=\vec{k}\ ,$$

$\vec{i}$, $\vec{j}$, $\vec{k}$ being unit vectors along the [100], [010], and [001] crystallographic axes. From the general formula giving $\mathcal{H}_{eq}$,[11,12] we get, in the cubic axes system,

$$\mathcal{H}_{eq}(D^1_0)=B^2_{4\,eq}(D^4_2-D^4_{-2})+B^2_{2\,eq}(D^2_2-D^2_{-2})\ ,$$

$$\mathcal{H}_{eq}(D^1_1)=-B^3_{4\,eq}D^4_3+B^{-1}_{4\,eq}D^4_{-1}+B^{-1}_{2\,eq}D^2_{-1}\ ,$$

$$\mathcal{H}_{eq}(D^1_{-1})=-B^{-1}_{4\,eq}D^4_1+B^3_{4\,eq}D^4_{-3}-B^{-1}_{2\,eq}D^2_1\ ,$$

with

$$\frac{B^{-1}_{4\,eq}}{B^3_{4\,eq}}=\frac{1}{\sqrt{7}}\ ,\qquad \frac{B^2_{4\,eq}}{B^3_{4\,eq}}=\frac{2}{\sqrt{7}}\ ,\qquad \frac{B^2_{2\,eq}}{B^{-1}_{2\,eq}}=\frac{1}{\sqrt{2}}\ ;$$

we can thus verify that $\mathcal{H}_{eq}(D^1_0)$, $\mathcal{H}_{eq}(D^1_1)$, and $\mathcal{H}_{eq}(D^1_{-1})$ transform, respectively, as T_{20}, T_{21}, and T_{2-1}.

It is well known that the $^6A_1$ level of a $3d^5$ ion can be coupled only with the $^4T_1$ levels by the spin-orbit interaction[13,14]; thus the dipole strength of a transition $\Gamma^*(^6A_1)\rightarrow\Gamma^{*\prime}(^4E)$ is given by a second-order perturbation:

$$\mathfrak{G}[\Gamma^*(^6A_1)\rightarrow\Gamma^{*\prime}(^4E)]=\sum_{(^6A_1)M_{\Gamma^*}}\ \sum_{(^4E)M_{\Gamma^{*\prime}}}\Big|\sum_{(^4_iT_1)\Gamma^*M_{\Gamma^*}J}\times\frac{\langle(^6A_1)\Gamma^*M_{\Gamma^*}|\mathcal{H}_{so}|(^4_iT_1)\Gamma^*M_{\Gamma^*}J\rangle\langle(^4_iT_1)\Gamma^*M_{\Gamma^*}J|\mathcal{H}_{eq}|(^4E)\Gamma^{*\prime}M_{\Gamma^{*\prime}}\rangle}{W(^6A_1)-W(^4_iT_1)}\Big|^2\ ,$$

with $\Gamma^*=\Gamma_7(^6A_1)$, $\Gamma_8(^6A_1)$ and $\Gamma^{*\prime}=\Gamma_6(^4E)$, $\Gamma_7(^4E)$, $\Gamma_8(^4E)$.

To obtain this relation we have used the facts that $\mathcal{H}_{so}$ and $\mathcal{H}_{eq}$ span, respectively, the A_1 and T_2 representations of the spinor group T_d^*. The products of matrix elements can be calculated easily since

$$\Omega_{JJ'}\begin{pmatrix}S & S' & T_1\\ T_1 & A_1 & \Gamma^*\end{pmatrix}=[3(2S+1)]^{-1/2}\delta(J,S)\delta(J',S).$$

The dipole strength of a transition $\Gamma\ (^6A_1)\rightarrow\Gamma'(^4A_1)$ is given by a third-order perturbation. Using the above notations we get

$$\mathfrak{G}[\Gamma^*(^6A_1)\rightarrow\Gamma_8(^4A_1)]=\sum_{(^6A_1)M_{\Gamma^*}}\ \sum_{(^4A_1)\Gamma_8M_{\Gamma^{*\prime}}}\Big|\sum_{(^4_iT_1)\Gamma^*M_{\Gamma^*}5/2}\ \sum_{(^4_jT_1)\Gamma_8M_{\Gamma^{*\prime},3/2}}\langle(^6A_1)\Gamma^*M_{\Gamma^*}|\mathcal{H}_{so}|(^4_iT_1)\Gamma^*M_{\Gamma^*}\tfrac{5}{2}\rangle$$

$$\times\langle(^4_iT_1)\Gamma^*M_{\Gamma^*}\tfrac{5}{2}|\mathcal{H}_{eq}|(^4_jT_1)\Gamma_8M_{\Gamma^{*\prime}},\tfrac{3}{2}\rangle\langle(^4_jT_1)\Gamma_8M_{\Gamma^{*\prime}},\tfrac{3}{2}|\mathcal{H}_{so}|(^4A_1)\Gamma_8M_{\Gamma^{*\prime}}\rangle$$

$$\times\frac{1}{[W(^6A_1)-W(^4_iT_1)][W(^4A_1)-W(^4_jT_1)]}+\sum_{(^4_iT_1)\Gamma^*M_{\Gamma^*}5/2}\ \sum_{(^4_jT_2)\Gamma^*M_{\Gamma^*}J}\langle(^6A_1)\Gamma^*M_{\Gamma^*}|\mathcal{H}_{so}|(^4_iT_1)\Gamma^*M_{\Gamma^*}\tfrac{5}{2}\rangle$$

$$\times\langle(^4_iT_1)\Gamma^*M_{\Gamma^*}\tfrac{5}{2}|\mathcal{H}_{so}|(^4_jT_2)\Gamma^*M_{\Gamma^*}J\rangle\langle(^4_jT_2)\Gamma^*M_{\Gamma^*}J|\mathcal{H}_{eq}|(^4A_1)\Gamma_8M_{\Gamma^{*\prime}}\rangle\frac{1}{[W(^6A_1)-W(^4_iT_1)][W(^4A_1)-W(^4_jT_2)]}\Big|^2\ .$$

The explicit calculation given in the Appendix shows that the dipole strength of a transition $\Gamma(^6A_1) \rightarrow \Gamma'(^4A_1)$ should be roughly 1000 times smaller than the dipole strength of a transition $\Gamma(^6A_1) \rightarrow \Gamma'(^4E)$. The band at 23 300 cm^{-1} is not sufficiently forbidden to be associated with the $^6A_1 \rightarrow {}^4A_1$ transition.

For Mn^{++} in ZnS it is known from EPR spectra that the levels $\Gamma_7(^6A_1)$ and $\Gamma_8(^6A_1)$ are separated by only 23.6×10^{-4} cm^{-1}.[15] This splitting cannot be observed in the optical spectra and will be neglected. Using the Ω's and the Π's we get the following relative dipole strengths for unpolarized light:

$$\mathcal{G}[^6A_1 \rightarrow \Gamma_6(^4E)] = 2\,, \quad \mathcal{G}[^6A_1 \rightarrow \Gamma_7(^4E)] = 3\,,$$

$$\mathcal{G}[^6A_1 \rightarrow \Gamma_8(^4E)] = 5\,.$$

In the case of a stressed crystal ($\vec{P} \parallel [1\bar{1}0]$), we must use the eigenvectors of the matrix of Sec. III C; they are given in Table V.

The components of the normalized eigenvectors will be noted (Γ^*, M_{Γ^*}) in the following. The dipole strengths $\mathcal{G}(\pi)$, for light polarized along the $[1\bar{1}0]$ crystallographic axis and the dipole strengths $\mathcal{G}(\sigma_1)$ for light polarized along the [110] crystallographic axis are given by

$$\mathcal{G}\left(\begin{matrix}\pi\\ \sigma_1\end{matrix}\right) = \tfrac{1}{20}\left|-(\Gamma_6+\tfrac{1}{2}) + 2(\Gamma_8+\tfrac{1}{2}) \pm i\sqrt{3}\,(\Gamma_7+\tfrac{1}{2})\right|^2$$
$$+\tfrac{1}{20}\left|3^{-1/2}(\Gamma_6-\tfrac{1}{2}) + \frac{4}{\sqrt{3}}(\Gamma_8+\tfrac{1}{2})\right.$$
$$\left.\mp 3i(\Gamma_7+\tfrac{1}{2}) \pm 2i(\Gamma_8-\tfrac{3}{2})\right|^2$$
$$+\tfrac{1}{12}\left|2(\Gamma_6+\tfrac{1}{2}) - (\Gamma_8+\tfrac{1}{2}) \pm i\sqrt{3}\,(\Gamma_8-\tfrac{3}{2})\right|^2,$$

where the upper signs correspond to $\mathcal{G}(\pi)$ and the lower signs to $\mathcal{G}(\sigma_1)$. For light polarized along the [001] crystallographic axis, we get

$$\mathcal{G}(\sigma_2) = \tfrac{2}{5}\left|(\Gamma_6+\tfrac{1}{2}) + (\Gamma_8+\tfrac{1}{2})\right|^2 + \tfrac{6}{10}\left|(\Gamma_7+\tfrac{1}{2}) + (\Gamma_8-\tfrac{3}{2})\right|^2.$$

To obtain these relations we neglected the mixing of the intermediate levels $|(^4_iT_1)\Gamma^* M_{\Gamma^*} J\rangle$ by the rhombic deformation, this hypothesis being correct if the spin-orbit interaction is stronger than ΔV.

E. Splitting of the ^4E Level in C_{3v} Symmetry

When pressure is applied along the [111] crystallographic axis, the symmetry is reduced from tetrahedral to trigonal. The nonzero linear combinations of the stress tensor are[6]

$$\epsilon(A_1) = (s_{11}+2s_{12})P\,,$$

$$\epsilon(T_{2\xi}) = \epsilon(T_{2\eta}) = \epsilon(T_{2\zeta}) = s_{44}P/3\,.$$

It must be noted that in this case, the three components of T_2 intervene, whereas in the case $\vec{P} \parallel [1\bar{1}0]$ only $T_{2\xi}$ intervenes.

TABLE V. Eigenvalues and coefficients of the eigenvectors of the matrix giving the splitting of the Γ_8 level and the shifts of the Γ_6 and Γ_7 levels. The coefficients correspond to unnormalized eigenvectors. The upper signs of the coefficients correspond to the upper signs given in the upper row. θ is defined by $\theta = \arctan(|Z|/X)$.

	$\Gamma_6 \pm \frac{1}{2}$	$\Gamma_7 \pm \frac{1}{2}$	$\Gamma_8 \mp \frac{3}{2}$	$\Gamma_8 \pm \frac{1}{2}$
$\lambda = +\frac{1}{2}\lvert Z\rvert$	$+1$	$\pm i$	$+i(+1+3/2\tan\theta)$	$\pm(-1+3/2\tan\theta)$
$\lambda = -\frac{1}{2}\lvert Z\rvert$	$+1$	$\mp i$	$+i(-1+3/2\tan\theta)$	$\mp(1+3/2\tan\theta)$
$\lambda = +\frac{3}{2}(X^2+\lvert Z\rvert^2)^{1/2}$	$\left(\frac{1}{\tan\theta} - \frac{1}{\sin\theta}\right)\left(\frac{27}{8\sin^2\theta} - \frac{3}{8}\right) + \frac{3}{2\sin\theta}$	$\pm i\left(\frac{9}{8\sin^2\theta} + \frac{3}{8}\right)$	$i\left[\frac{3}{4} + \frac{3}{2\sin\theta}\left(\frac{3}{2\tan\theta} - \frac{3}{2\sin\theta}\right)\right]$	$\pm\left(\frac{-3}{2\sin\theta} + \frac{3}{4\tan\theta}\right)$
$\lambda = -\frac{3}{2}(X^2+\lvert Z\rvert^2)^{1/2}$	$\left(\frac{1}{\tan\theta} + \frac{1}{\sin\theta}\right)\left(\frac{27}{8\sin^2\theta} - \frac{3}{8}\right) - \frac{3}{2\sin\theta}$	$\pm i\left(\frac{9}{8\sin^2\theta} + \frac{3}{8}\right)$	$i\left[\frac{3}{4} - \frac{3}{2\sin\theta}\left(\frac{3}{2\tan\theta} + \frac{3}{2\sin\theta}\right)\right]$	$\pm\left(\frac{3}{2\sin\theta} + \frac{3}{4\tan\theta}\right)$

Under C_{3v} symmetry, the ^4E level decomposes into four distinct levels:

$$(^4E)_{C_{3v}} \rightarrow 3\Gamma_4 + \{\Gamma_5 + \Gamma_6\} ,$$

(levels Γ_5 and Γ_6 are degenerate, being related by time-reversal symmetry). We calculated the splittings in the trigonal axis system, $[1\bar{1}2]$, $[\bar{1}10]$, and $[111]$, using complex basis functions.

In this axis system the variation of the crystal field is given by

$$\Delta V_{C_{3v}} = (\Delta B_2^0 D_0^2 + \Delta B_4^0 D_0^4) s_{44} P/3 .$$

D_q^k's are tensor operators defined by Judd.[16] The matrix elements of $\mathcal{H}_{so} + \Delta V_{C_{3v}}$ were calculated from the eigenfunctions of $\mathcal{H}_c$ expressed in the trigonal axis system. They are given in Table VI where

$$A = 2e^{i\pi/2} Y , \qquad B = -2\sqrt{6}\, e^{3i\pi/4} Y ,$$

$$C = 2\sqrt{2}\, e^{i\pi/4} Y ,$$

$$Y = \frac{5\sqrt{3}}{189} \rho s_{44} P \left(\sum \frac{\beta_i^2}{\Delta_i} \left(\tfrac{1}{7} \langle r^2 \rangle \Delta B_2^0 + \tfrac{13}{189} \langle r^4 \rangle \Delta B_4^0 \right) \right.$$

$$+ \sum \frac{\alpha_i \beta_i}{\Delta_i} \left(\tfrac{2}{27} \langle r^4 \rangle \Delta B_4^0 \right)$$

$$\left. + \sum \frac{\beta_i'^2}{\Delta_i} \left(\tfrac{1}{35} \langle r^2 \rangle \Delta B_2^0 - \tfrac{1}{63} \langle r^4 \rangle \Delta B_4^0 \right) \right) ,$$

and

$$U = \tfrac{10}{21} (s_{44} P)^2 \left(\tfrac{1}{49} \sum \frac{\beta_i^2}{\Delta_i} (\langle r^2 \rangle \Delta B_2^0 + \tfrac{13}{27} \langle r^4 \rangle \Delta B_4^0)^2 \right.$$

$$+ \tfrac{4}{729} \sum \frac{\beta_i^2}{\Delta_i} (\langle r^4 \rangle \Delta B_4^0)^2$$

$$+ \tfrac{4}{189} \sum \frac{\alpha_i \beta_i}{\Delta_i} (\langle r^2 \rangle \Delta B_2^0 + \tfrac{13}{27} \langle r^4 \rangle \Delta B_4^0)(\langle r^4 \rangle \Delta B_4^0)$$

$$\left. + \tfrac{5}{441} \sum \frac{\beta_i'^2}{\Delta_i} (-\tfrac{1}{5} \langle r^2 \rangle \Delta B_2^0 + \tfrac{1}{9} \langle r^4 \rangle \Delta B_4^0)^2 \right) .$$

TABLE VI. Matrix elements of the pressure-induced crystal field and of the spin-orbit interaction when $\vec{P} \parallel [111]$. U, A, B, and C are defined in Sec. III E. X is defined in Sec. III C.

	$\Gamma_6 \frac{1}{2}$	$\Gamma_7 \frac{1}{2}$	$\Gamma_8 - \frac{3}{2}$	$\Gamma_8 \frac{1}{2}$	$\Gamma_6 - \frac{1}{2}$	$\Gamma_7 - \frac{1}{2}$	$\Gamma_8 \frac{3}{2}$	$\Gamma_8 - \frac{1}{2}$
$\Gamma_6 \frac{1}{2}$	$-\frac{3}{2}X + U$	A	$-2A$	0	0	C	$-C$	B
$\Gamma_7 \frac{1}{2}$		$\frac{3}{2}X + U$	0	$-2A$	$-C$	0	$-B$	$-C$
$\Gamma_8 - \frac{1}{2}$			U	A	$-C$	$-B$	0	$-C$
$\Gamma_8 \frac{1}{2}$				U	B	$-C$	C	0
$\Gamma_6 - \frac{1}{2}$					$-\frac{3}{2}X + U$	$-A$	$-2A$	0
$\Gamma_7 - \frac{1}{2}$						$\frac{3}{2}X + U$	0	$-2A$
$\Gamma_8 \frac{3}{2}$	(complex conjugate)						U	$-A$
$\Gamma_8 - \frac{1}{2}$								U

TABLE VII. Contribution of the levels $^4T_1$, $^4T_2$, $^2T_1$ and $^2T_2$ to the splitting of the ^4E level for $P = 0$. The Racah parameters and Dq are given in Sec. IV. Δ measures the separation between the Γ_6 and Γ_7 levels [$\Delta = W(\Gamma_6) - W(\Gamma_7)$].

Level[a]	Energy (cm^{-1})	Level[a]	Energy (cm^{-1})	Level[a]	Energy (cm^{-1})
$(P)\ ^2T_1$	66 680	$(D_1)\ ^2T_2$	72 130	$(F)\ ^4T_1$	35 300
$(G_1)\ ^2T_1$	53 520	$(G_1)\ ^2T_2$	53 900	$(P)\ ^4T_1$	26 130
$(F_2)\ ^2T_1$	40 940	$(D_2)\ ^2T_2$	49 290	$(G)\ ^4T_1$	18 410
$(G_2)\ ^2T_1$	39 480	$(F_2)\ ^2T_2$	41 590	Contribution to Δ 2.08 cm^{-1}	
$(H)\ ^2_aT_1$	38 240	$(G_2)\ ^2T_2$	40 120		
$(H)\ ^2_bT_1$	36 640	$(H)\ ^2T_2$	38 790	$(F)\ ^4T_2$	36 470
$(F_1)\ ^2T_1$	33 330	$(F_1)\ ^2T_2$	34 360	$(D)\ ^4T_2$	24 980
$(I)\ ^2T_1$	29 000	$(D_3)\ ^2T_2$	32 440	$(G)\ ^4T_2$	20 870
Contribution to Δ -15.09 cm^{-1}		$(I)\ ^2_aT_2$	29 660	Contribution to Δ 0.16 cm^{-1}	
		$(I)\ ^2_bT_2$	26 850		
		Contribution to Δ 25.88 cm^{-1}			

[a]Levels are labeled following the convention of Griffith (Ref. 8) and J. C. Slater [*Quantum Theory of Atomic Structures* (McGraw-Hill, New York, 1960), Vol. 2].

IV. RESULTS AND DISCUSSION

A. Splitting of ^4E Level for Zero Applied Pressure

The computed contributions of all the $^2T_1$, $^4T_1$, $^2T_2$, and $^4T_2$ levels to the splitting of the ^4E level are given in Table VII. The energies of the spectroscopic terms were deduced from the following values of the Racah coefficients:

$$B = 730\ cm^{-1} , \quad C = 2880\ cm^{-1} .$$

The matrix elements of the cubic crystal field between the spectroscopic terms were calculated from the following value of the cubic field parameter:

$$Dq = -420\ cm^{-1} .$$

The length of the calculation was slightly reduced by noting that the matrix elements of an even crystal field operator are zero when they are diagonal in the seniority. The larger matrix that we obtained was the 10×10 matrix giving the $^2T_2$ states. The matrix elements of the spin-orbit interaction were calculated by taking $\rho = 300\ cm^{-1}$.

Of course, there is some uncertainty on the theoretical results because the parameters B, C, and Dq are not well defined from the experimental levels[3,4] and because most of the calculated energy levels cannot be compared with experiment. In fact, at least for the $^4T_1$ and $^4T_2$ levels, the results do not depend strongly on B, C, and Dq; the splitting calculated from the values chosen in a preceding paper[12] and from the values given here differ by no more than 10%.

The following general features can be deduced from Table VII: (i) The contribution of the $^4T_2$ levels is negligible, $W(\Gamma_6) - W(\Gamma_7) < 0.2$ cm^{-1}. (ii) The contribution of the $^2T_1$ levels and the contribution of the $^2T_2$ levels are preponderant.

The over-all contribution to the splittings gives

$$W(\Gamma_6) = -W(\Gamma_7) = 9.18 \text{ cm}^{-1} ,$$

the Γ_8 level being taken as reference. This value compares favorably with the experimental value of the splitting (4.5 cm^{-1}).

B. Splitting, Shifts, and Polarization in the Case $\vec{P} \parallel [1\bar{1}0]$

First, we shall study the splitting of the Γ_8 level and the shifts of the other lines with respect to their center of gravity. In an ionic model, the center of gravity of the cubic lines ^4E is not shifted linearly by the hydrostatic component of the stress [Fig. 1(a)]. Detailed calculations taking into account covalency could explain the observed linear shift.[6] Knowing the experimental value of X from the splittings obtained for $\vec{P} = 0$, we can deduce the experimental value of Z by fitting the observed shifts and splittings (see Fig. 3). We get

$$|Z|_{\text{expt}} = 23 \times 10^{-10} \text{ cm}^{-1}/(\text{dyn/cm}^2) .$$

In order to calculate Z, the part of ΔV spanning T_{20} will be written in terms of tensor operators $D_p^{(t)}$ defined by Judd[16]:

$$\Delta V(T_{20}) = +[\Delta B_2^2 (D^2_{-2} - D_2^2) + \Delta B_4^2 (D^4_{-2} - D_2^4)] \epsilon(T_{2\xi}).$$

Evaluating the relevant matrix elements of $\Delta V(T_{20})$, we get

$$Z = -\tfrac{2}{441}\sqrt{15}\,\rho\epsilon(T_{2\xi})\Big(+\sum \frac{\beta_i^2}{\Delta_i}\,(2\sqrt{30}\,\langle r^2\rangle \Delta B_2^2 + \tfrac{13}{3}\sqrt{2}\,\langle r^4\rangle \Delta B_2^4) + \sum_i \frac{\alpha_i \beta_i}{\Delta_i}\,\tfrac{14}{3}\sqrt{2}\,\langle r^4\rangle \Delta B_2^4 + \sum \frac{\beta_i'^2}{\Delta_i'}\,(\tfrac{2}{5}\sqrt{30}\,\langle r^2\rangle \Delta B_2^2 - \sqrt{2}\,\langle r^4\rangle \Delta B_2^4)\Big) .$$

In a point-charge model ΔB_2^2 and ΔB_2^4 are given by

$$\Delta B_2^2 = -i\tfrac{4}{9}\sqrt{6}\, e\, e_{\text{eff}}/R^3$$

and

$$\Delta B_2^4 = i\tfrac{10}{9}\sqrt{10}\, e\, e_{\text{eff}}/R^5 ,$$

e and e_{eff} being, respectively, the charge of the electron and the effective charge of the nearest neighbors. R is the anion-cation distance; $\langle 3d|r^4|3d\rangle\, \Delta B_4^2$ can be deduced from the experimental value of the cubic field parameter by

$$(e\, e_{\text{eff}}/R^5)\langle 3d|r^4|3d\rangle = -\tfrac{27}{2} Dq .$$

To our knowledge there is no experimental measure of $(e\, e_{\text{eff}}/R^3)\langle 3d|r^2|3d\rangle$; we will therefore use a relation given by Blume and Orbach[13]:

$$\langle 3d|r^2|3d\rangle = 0.28\,\langle 3d|r^4|3d\rangle/a_0^2 ,$$

a_0 being the first Bohr radius. From $Dq = -420$ cm^{-1}, $s_{44} = 0.243 \times 10^{-11}$ cm^2/dyn,[17] and $\rho = 300$ cm^{-1}, we obtain

$$Z = 2.62 \times 10^{-10} \text{ cm}^{-1}/(\text{dyn/cm}^2) .$$

Given the crudeness of the model used to obtain this value, we could not hope for more than order-of-magnitude agreement with experiment.

Up to now the existence of two cubic sites in our crystal was not taken into account, these sites being equivalent for $\vec{P} \parallel [1\bar{1}0]$. In fact, we have verified by EPR experiments on the determination of the spin-lattice coupling coefficients of Mn^{++} in ZnS,[18,19] that these coefficients do not depend on the presence of two cubic sites, or on the presence of a small quantity of hexagonal or more complex sites, this indicating that the pressure-induced deformations can be calculated independently for each center.

However, for polarization studies, the relative positions of the two cubic sites intervene. We can obtain one site by rotating the other by 180° around a [111] crystallographic axis denoted $[111]_W$ (Fig. 5).

In our experiments, the light beam was in the plane $(1\bar{1}0)_W$ and made an angle $\theta = 27°$ with the $[111]_W$ axis. With α denoting the angle between the axis $[111]_W$ and $[001]'$ we get

$$\mathcal{G}(\vec{E} \parallel \vec{P}) = 2\mathcal{G}(\Pi)$$

for light polarized parallel to $\vec{P}$, and

$$\mathcal{G}(\vec{E} \perp \vec{P}) = \mathcal{G}_1[\cos^2(\alpha - \theta) + \cos^2(\alpha - \theta)] + \mathcal{G}_2[\sin^2(\alpha - \theta) + \sin^2(\alpha + \theta)]$$

for light polarized perpendicular to $\vec{P}$. The relative dipole strengths were calculated for $P = 16 \times 10^8$ dyn/cm^2.

The experimental conditions do not permit a di-

TABLE VIII. Theoretical dipole strengths for $P = 16 \times 10^8$ dyn/cm^2 ($\vec{P} \parallel [1\bar{1}0]$). The lines are determined by the eigenvalues of the matrix given in Sec. III C. The values given in parentheses are obtained by taking into account the mixing of the $^4T_1$ levels via the rhombic deformations.

Eigenvalue	$+\frac{3}{2}(X^2 + \lvert Z\rvert^2)^{1/2}$ line at higher energy	$+\frac{1}{2}\lvert Z\rvert$	$-\frac{1}{2}\lvert Z\rvert$	$-\frac{3}{2}(X^2 + \lvert Z\rvert^2)^{1/2}$ line at lower energy
Dipole strengths $\vec{E} \parallel \vec{P}$	1.0	0.65	0.10	0.25
	(1.06)	(0.64)	(0.10)	(0.18)
Dipole strengths $\vec{E} \perp \vec{P}$	0.26	0.44	0.64	0.38
	(0.28)	(0.56)	(0.60)	(0.52)

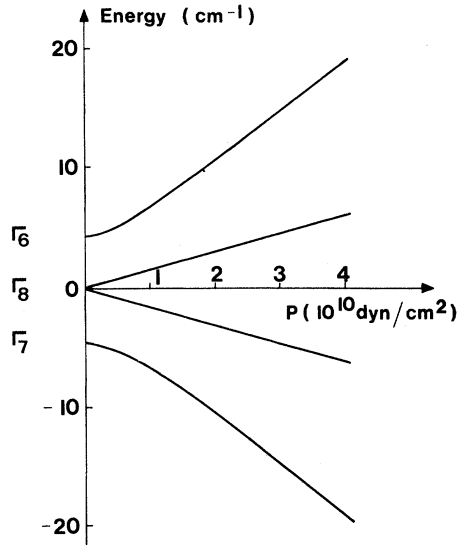

FIG. 8. Theoretical splitting as a function of applied pressure. Pressure $\vec{P} \parallel [111]_W$.

rect comparison between the spectra shown in Fig. 4 obtained for light polarized parallel to $\vec{P}$ and for light polarized perpendicular to $\vec{P}$, the spectra being attenuated by a factor 2.2 for light polarized parallel to $\vec{P}$. The theoretical values are reported in Table VIII; the values obtained from the hypothesis of a slight mixing of the intermediate levels $\Gamma_7(^4T_1)$ and $\Gamma_8(^4T_1)$ by rhombic distortions are given in brackets. These values describe correctly the polarization effects, in particular, the relatively small dipole strength of the two lines at higher energy when $\vec{E} \perp \vec{P}$; however, the theoretical dipole strength for one of the two lines at lower energy seems to be too small. We must note that the polarization effects are identical for the groups A and C (in Fig. 4, the resolution is better for group A than for group C, this explaining the broadening of the lines).

C. Splitting and Shift in the Case $\vec{P} \parallel [111]$: Mn^{++} in Wurtzite

In the axis system defined in Sec. III E, the amplitudes of the relevant pressure-induced crystal field components are

$$\Delta B_2^0 = \tfrac{8}{3} e\, e_{eff}/R^3$$

and

$$\Delta B_4^0 = 10\, e\, e_{eff}/R^5 .$$

The shift of the center of gravity of the levels is proportional to the square of the applied pressure:

$$U = -6.6\times 10^{-20} P^2 .$$

Y is given by

$$Y = 0.3\times 10^{-10} P .$$

(U and Y are expressed in cm^{-1} and P is expressed in dyn/cm^2.) The computed relative positions of the levels are given in terms of applied pressure in Fig. 8. For $P = 36\times 10^8$ dyn/cm^2, the theoretical splitting of the Γ_8 level is roughly 1 cm^{-1}. This splitting can hardly be observed experimentally (Fig. 6).

For Mn^{++} in wurtzite the theoretical splitting of the central line is roughly 3 cm^{-1}. (In this case we calculated U and Y in terms of the noncompensated cubic part of the crystal field defined by Sharma *et al.*[20])

Since all lines of groups B and C are equally sharp, they cannot be associated with Mn^{++} in wurtzite. Furthermore these lines do not exhibit significant polarization effects for zero applied pressure.

V. CONCLUSION

We have shown that the three lines of each group A, B, and C are associated with the $\Gamma_6(^4E)$, $\Gamma_7(^4E)$, and $\Gamma_8(^4E)$ levels of Mn^{++} in cubic ZnS. By studying the splitting of the ^4E and $^4A_1$ levels and the dipole strengths of the $(^6A_1) \rightarrow (^4A_1)$ and $(^6A_1) \rightarrow (^4E)$ transitions, we have shown that the $^4A_1$ level cannot intervene in the description of the observed fine structures and that the $(^6A_1) \rightarrow (^4A_1)$ transition is very strongly forbidden.

ACKNOWLEDGMENTS

We would like to express our sincere thanks to Professor J. Hervé and Professor J. Mattler for their deep interest in this work. We are indebted to C. Naud for assistance with the experiments. Thanks are due to N. Machorine, F. Buraud, and P. Villermet for cutting and polishing the samples used in the experiments.

APPENDIX

Neglecting the splitting of the $\Gamma_7(^6A_1)$ and $\Gamma_8(^6A_1)$ levels, we obtain the following dipole strengths:

$$\mathcal{G}[(^6A_1) \rightarrow (^4A_1)] = 6\rho^4 N^2 \left(\left| -\tfrac{2}{63}\sqrt{15}\,\langle r^2\rangle B^2_{2\,eq} + \tfrac{5}{126}\langle r^4\rangle B^2_{4\,eq} \right|^2 \right.$$

$$\left. + \left| -\tfrac{2}{21}\sqrt{3}\,\langle r^2\rangle B^2_{2\,eq} + \tfrac{1}{42}\sqrt{5}\,\langle r^4\rangle B^2_{4\,eq} \right|^2 + \left| +\tfrac{7}{32}\sqrt{3}\,\langle r^2\rangle B^2_{2\,eq} - \tfrac{1}{14}\sqrt{5}\,\langle r^4\rangle B^2_{4\,eq} \right|^2 \right) ,$$

with

$$N=\frac{\sqrt{30}}{2}\sum_i \frac{\alpha_i\gamma_i}{W(^6A_1)-W(^4_iT_1)}\sum_i \frac{\beta_i'^2}{W(^4A_1)-W(^4_iT_2)}+\frac{4\sqrt{42}}{7}\sum_i \frac{\alpha_i\beta_i}{W(^6A_1)-W(^4_iT_1)}\sum_i \frac{\alpha_i'\beta_i'}{W(^4A_1)-W(^4_iT_2)}$$

$$-\frac{5\sqrt{14}}{14}\sum_i \frac{\alpha_i\beta_i}{W(^6A_1)-W(^4_iT_1)}\sum_i \frac{\beta_i'\gamma_i'}{W(^4A_1)-W(^4_iT_2)}+\sqrt{42}\sum_i \frac{\alpha_i^2}{W(^6A_1)-W(^4_iT_1)}\sum_i \frac{\alpha_i'\beta_i'}{W(^4A_1)-W(^4_iT_2)}$$

and

$$\mathcal{G}[(^6A_1)\rightarrow\Gamma_7(^4E)]\ 9\rho^2\Big|\sum_i \frac{\alpha_i\beta_i}{W(^6A_1)-W(^4_iT_1)}\left(\tfrac{3}{735}\sqrt{210}\,\langle r^2\rangle B^2_{2\,eq}+\tfrac{13}{147}\sqrt{14}\,\langle r^4\rangle B^2_{4\,eq}\right)$$

$$+\sum_i \frac{\alpha_i^2}{W(^6A_1)-W(^4_iT_1)}\left(\tfrac{2}{21}\sqrt{14}\,\langle r^4\rangle B^2_{4\,eq}\right)\Big|^2 .$$

The α_i, β_i, γ_i, α_i', β_i', γ_i' are defined in Sec. III B. The ratio $\langle r^2\rangle B^2_{2\,eq}/\langle r^4\rangle B^2_{4\,eq}=9\sqrt{3}/\sqrt{5}$ can be easily calculated from the general relations giving the equivalent even fields.[12] Numerical calculation gives

$$\frac{\mathcal{G}[(^6A_1)\rightarrow(^4A_1)]}{\mathcal{G}[(^6A_1)\rightarrow\Gamma_7(^4E)]}=6.5\times10^{-3} .$$

[1]L. E. Orgel, J. Chem. Phys. 23, 1004 (1955).

[2]S. Sugano and Y. Tanabe, J. Phys. Soc. Japan 9, 753; 9, 766 (1954).

[3]D. Langer and S. Ibuki, Phys. Rev. 138, A809 (1965).

[4]D. Langer and H. J. Richter, Phys. Rev. 146, 554 (1966).

[5]S. Koide and M. H. L. Pryce, Phil. Mag. 3, 607 (1958) 3, 607 (1958).

[6]A. I. Schawlow, A. H. Piksis, and S. Sugano, Phys. Rev. 122, 1469 (1961).

[7]C. Blanchard and R. Parrot, Solid State Commun. 10, 413 (1972).

[8]J. S. Griffith, *The Irreducible Tensor Method for Molecular Symmetry Groups* (Prentice-Hall, Englewood Cliffs, N. J., 1962).

[9]J. S. Griffith, *The Theory of Transition Metal Ions* (Cambridge U.P., Cambridge, England, 1964).

[10]M. H. L. Pryce, Phys. Rev. 80, 1107 (1950).

[11]A. Kiel, Phys. Rev. 148, 247 (1966).

[12]R. Parrot and C. Blanchard, Phys. Rev. B5, 819 (1972).

[13]M. Blume and R. Orbach, Phys. Rev. 127, 5 (1962).

[14]R. R. Sharma, T. P. Das, and R. Orbach, Phys. Rev. 149, 257 (1966).

[15]J. Schneider, S. R. Sircar, and A. Räuber, Z. Naturforsch. 18a, 980 (1963).

[16]B. R. Judd, Phys. Rev. 127, 750 (1962).

[17]*Selected Constants Relative to Semi-Conductors* (Pergamon, New York, 1961).

[18]R. Parrot, C. Blanchard, and D. Boulanger, Phys. Letters 34A, 109 (1971).

[19]C. Blanchard, R. Parrot, and D. Boulanger, Phys. Letters 36A, 179 (1971).

[20]R. R. Sharma, Phys. Rev. B 3, 76 (1971).

PHYSICAL REVIEW B VOLUME 6, NUMBER 10 15 NOVEMBER 1972

Symmetry of the Far-Infrared Resonant-Pair Mode in KCl : NaCl†

T. L. Templeton and B. P. Clayman

Department of Physics, Simon Fraser University, Burnaby, British Columbia, Canada

(Received 12 May 1972)

The symmetry of the far-infrared- (44-cm^{-1}) active resonant Na^+-Na^+ pair mode in KCl : NaCl has been determined by stress experiments to be tetragonal.

I. INTRODUCTION

Impurity pair modes have been observed in the allowed phonon bands of several alkali-halide systems: a single infrared-active absorption at 44 cm^{-1} due to Na^+-Na^+ pairs in KCl: NaCl,[1] a Raman-active scattering peak at 47 cm^{-1} due to Ag^+-Ag^+ pairs in NaCl:AgCl,[2] and, most recently, five infrared-active absorption lines at 32.7, 38.0, 40.2, 44.7, and 48.4 cm^{-1} due to F^--F^- pairs in NaCl:NaF.[3] A knowledge of the site symmetries is essential to an understanding of these pair modes.

By applying uniaxial stress to KCl:NaCl single crystals along the high-symmetry directions, the Na^+-Na^+ pair-mode frequency is observed to shift